nature materials

OCTOBER 2010 VOL 9 NO 10
www.nature.com/naturematerials

Boundary rules for actin

PRESSURE SENSORS
Rivals to human skin

MAGNETOELECTRICS
Room-temperature operation

SCIENCE IN MEXICO
The long road to progress

nature materials

LETTERS

PUBLISHED ONLINE: 19 SEPTEMBER 2010 | DOI: 10.1038/NMAT2855

Nucleation geometry governs ordered actin networks structures

Anne-Cécile Reymann[1], Jean-Louis Martiel[1,2], Théo Cambier[1], Laurent Blanchoin[1], Rajaa Boujemaa-Paterski[1]* and Manuel Théry[1]*

Actin filaments constitute one of the main components of cell cytoskeleton. Assembled into bundles in filopodia or in stress fibres, they play a pivotal role in eukaryotes during cell morphogenesis, adhesion and motility. The bundle emergence has been extensively related to specific actin regulators[1–3] *in vivo*[4–7]. Such dynamic modulation was also highlighted by biochemical reconstitution of the actin-network assembly, in bulk solution or with biomimetic devices[8–18]. However, the question of how geometrical boundaries, such as those encountered in cells, affect the dynamic formation of highly ordered actin structures remains poorly studied[14,19]. Here we demonstrate that the nucleation geometry in itself can be the principal determinant of actin-network architecture. We developed a micropatterning method that enables the spatial control of actin nucleation sites for *in vitro* assays. Shape, orientation and distance between nucleation regions control filament orientation and length, filament–filament interactions and filopodium-like bundle formation. Modelling of filament growth and interactions demonstrates that basic mechanical and probabilistic laws govern actin assembly in higher-order structures.

In cells, actin nucleation occurs at various locations at the plasma membrane, and bundles of parallel actin filaments are initiated at focal adhesion sites[1] or result from the rearrangement of the dynamic branched actin network of the lamellipodium[6]. Here, we modulate the positioning of nucleation sites at scales corresponding to cellular dimensions. As a first step and to precisely regulate the position of actin nucleation sites *in vitro*, we used a recently developed ultraviolet-based micropatterning approach[20] to create a template for the localization of the nucleation promoting factor pWA (Fig. 1a). pWA comprises the C-terminal domains from the WASP/Scar proteins, a ubiquitous family of proteins that initiate actin polymerization on a pre-existing actin filament in the presence of the Arp2/3 complex and an actin monomer[21–23]. A small volume of solution made of a minimal set of purified proteins ensuring actin polymerization[8,10] was placed between the pWA-coated micropatterned slide and a glass support. Functionalized micropatterns specifically initiate actin filament nucleation on their surface and promote two-dimensional growth of actin filaments (Fig. 1b). Real-time visualization of actin-filament nucleation and growth highlighted the autocatalytic process of network formation (see Supplementary Fig. S1). These networks consist of filaments growing from the pWA-coated regions, with their fast-growing, barbed end oriented outwards (Fig. 1c and Supplementary Fig. S2 and Videos S1–S3). In agreement with actin-filament growth on glass rods[15], as the nucleation waves propagate, dense and interconnected networks are formed on the micropattern (Supplementary Fig. S1). Collectively, actin filaments emanating from this dense meshwork self-organize normally to the micropattern edge, except within the narrow region close to the bar end (Fig. 1c,d). Although densely organized into a parallel network, these filaments can be further gathered into larger bundles by the addition of cross-linking factors; we therefore refer to them as filaments rather than bundles. We term as bundles the structures unaffected by the subsequent addition of cross-linkers (see Supplementary Fig. S6a and Video S5). We validated that filament growth on the micropattern was sensitive to known biochemical parameters: filament length increased with the concentration of G-actin, and reduced with increasing concentrations of Arp2/3 or capping protein. In addition, these filaments are bundled by α-actinin or fascin (see Supplementary Figs S1 and S6).

We took advantage of the geometrical control of actin growth to investigate the interaction between two sets of actin filaments growing toward each other. We therefore analysed actin growth from individual, concentric or eccentric circles. Twenty- to thirty-micrometre-long actin filaments grew radially inwards and outwards (Fig. 2a). Surprisingly, the networks generated by three concentric circles spaced 15 μm apart did not simply superimpose and the centripetal arrangement of parallel bundles disappeared. Instead, the interactions between inward- and outward-growing filaments formed short and thin antiparallel bundles between adjacent circles. Interestingly, actin-filament elongation seemed to be blocked by the presence of the dense actin network formed on the adjacent circles. To verify this, we quantified the local actin-network density by averaging several images taken separately on identical micropatterns (Fig. 2b). In addition, to understand how actin-filament growth could lead to these actin density profiles, we carried out numerical simulations, where actin filaments were nucleated with a constant linear density along the circle (see Supplementary Fig. S3 and Equations). Filaments grew normally out of the circle and their length was determined by the biochemical conditions. Actin filaments were then allowed or not to cross adjacent nucleation regions (see Supplementary Fig. S3), and theoretical density maps were derived from the local density of simulated actin filaments (Fig. 2b). Numerical simulations showed that, on concentric circles, filaments did not cross the dense network region lying on their path. Conversely, when the distance between separate nucleation regions was reduced, as in the case of eccentric circles, the density within the inner circle was no longer isotropic. Numerical simulations confirmed that extra filaments enter this innermost region to locally increase fluorescence intensity (Fig. 2b). This demonstrates that short, and thus stiff, filaments can grow through the dense network whereas longer and more

[1]Institut de Recherches en Technologies et Sciences pour le Vivant, iRTSV, Laboratoire de Physiologie Cellulaire et Végétale, CNRS/CEA/INRA/UJF, Grenoble, 38054, France, [2]Laboratoire Techniques de l'Ingénierie Médicale et de la Complexité, CNRS/UJF, Pavillon Taillefer Faculté de Médecine, La Tronche, 38706, France. *e-mail: rajaa.paterski@cea.fr; manuel.thery@cea.fr.

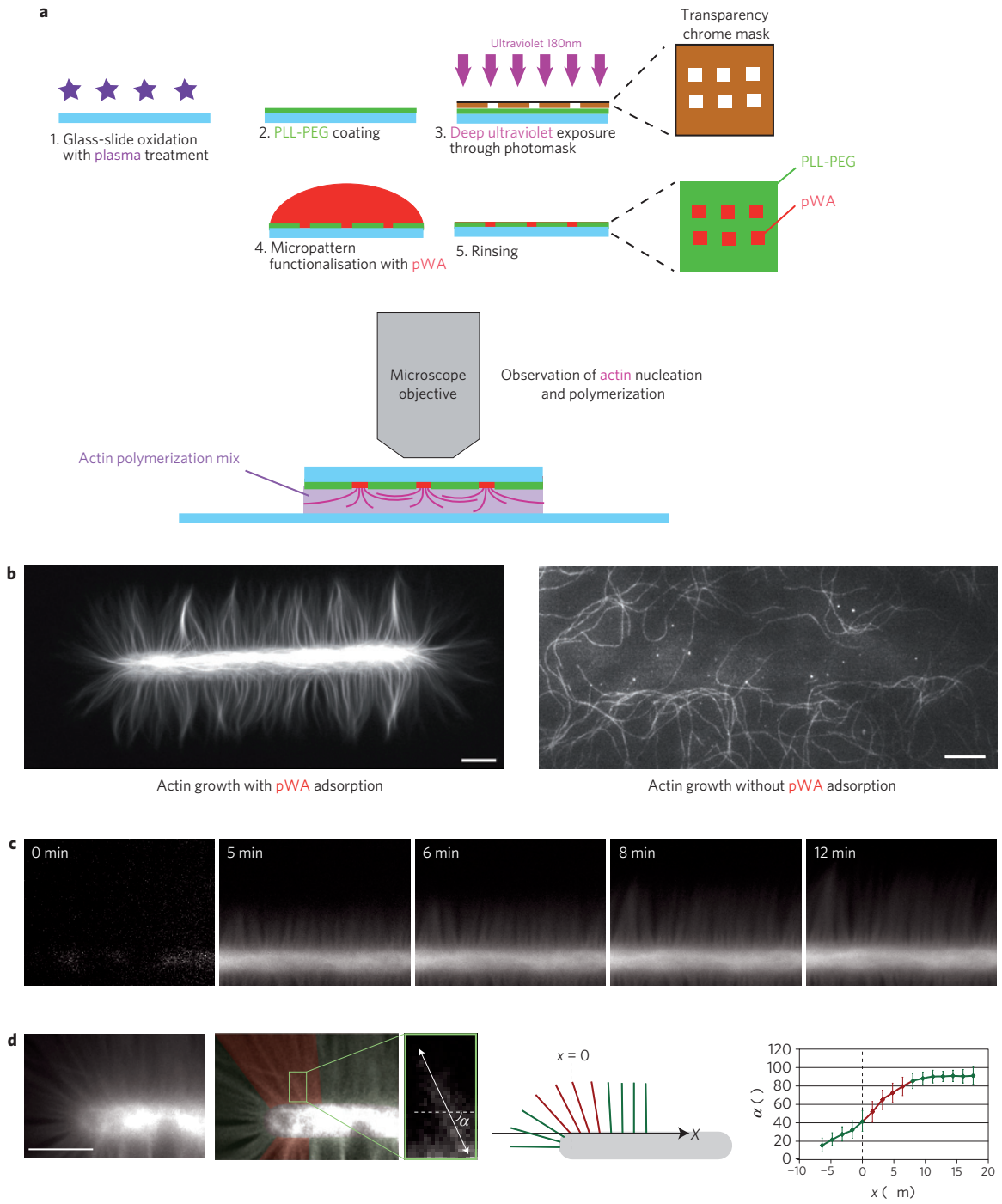

Figure 1 | Geometrical control of actin nucleation and growth. a, Surface-micropatterning method. **b**, Epifluorescence-microscopy images of actin filaments specifically nucleated on the pWA-coated micropattern, and of spontaneous filament polymerization in the solution in the absence of pWA-coating—no actin filament is recruited to the uncoated micropattern. **c**, Actin-filament nucleation and growth on a pWA-coated micropattern. **d**, The fluorescence image is filtered and the angle between the actin filament and the bar micropattern major axis manually measured with respect to their position (x) along the bar. The error bars (rightmost panel) represent the standard deviation calculated for 65 angles measured at each position (x). Filaments normal to the pattern edges are coloured green, and filaments of the transition region red. Scale bars indicate 10 μm. See also Supplementary Videos S1–S3.

flexible filaments become entangled and blocked by an adjacent actin network. Consequently, physical constraints in addition to biochemical cues regulate actin-filament length.

To further explore the role of geometrical parameters on actin-filament interactions and their resulting network structure, we forced contacts between filaments at various angles. When nucleated from two short bars, filaments first grew perpendicularly to the bars, then interacted and zipped to form a filopodium-like parallel bundle (Fig. 3a, see Supplementary Fig. S4 and Video S4), reminiscent of that present *in vivo*[6]. This interaction forced the filaments to bend, so bundle formation depended on filaments' ability to change their growing direction. We tested this parameter by varying the angle between the two short bars (Fig. 3b) and quantified the formation of parallel bundles (Fig. 3c). For

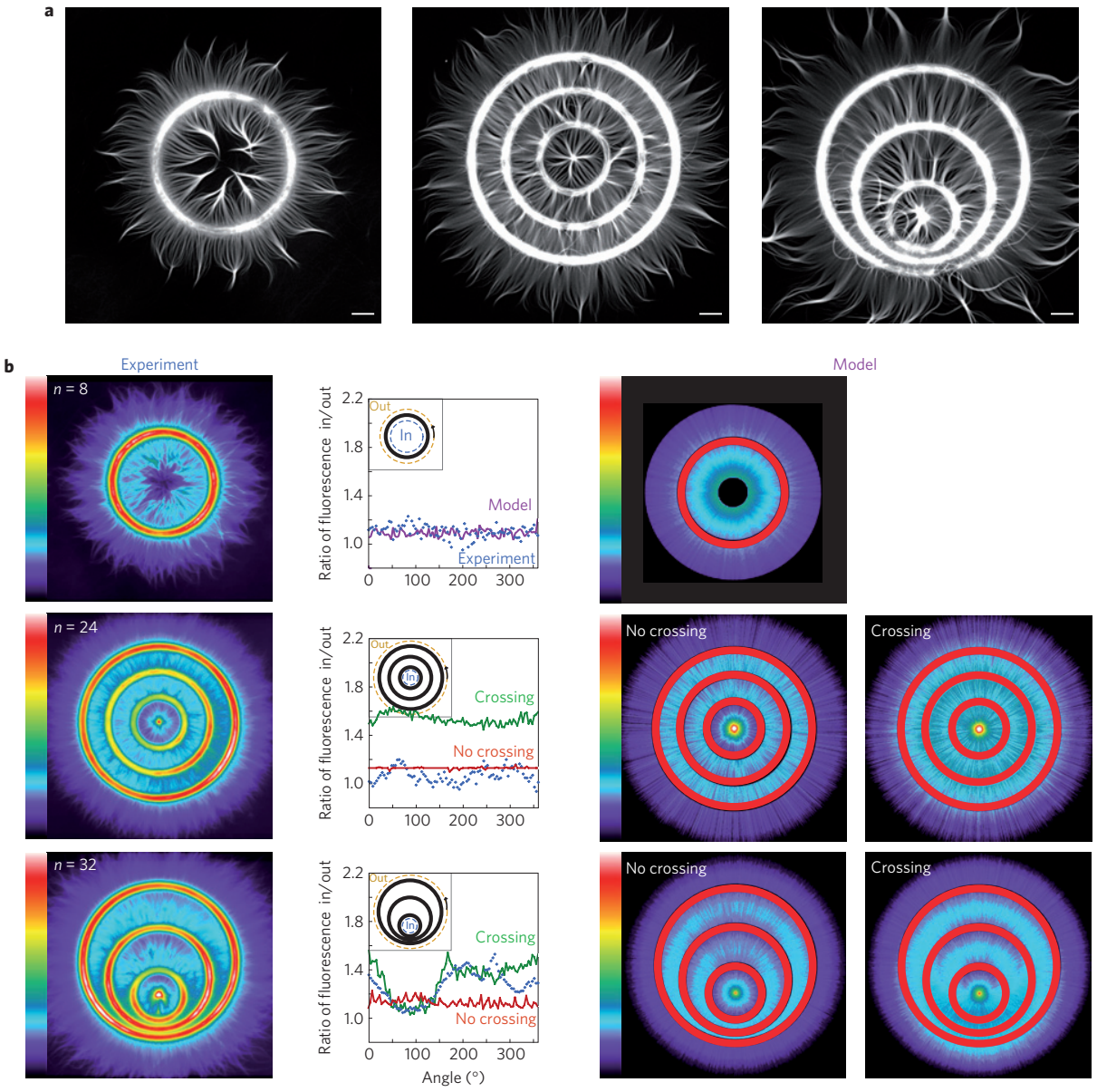

Figure 2 | Filament length controls their ability to cross dense actin networks. a, Fluorescent-microscopy images of actin structures formed on nucleation circles. Inward-growing filaments were brought together by the circle curvature and generated parallel bundles. **b**, Actin-network density maps calculated by overlaying and averaging several images (first column) and from numerical simulations of actin-filament growth (third and fourth columns). The averaged structure was colour-coded (see also Supplementary Fig. S3) and nucleation regions are represented in red. We measured the fluorescence ratio of line scans along the innermost circle and the external side of the outermost circle (as a reference) as in the inset image (second column, coloured dashed circles). The second column shows the comparison between the ratios of the experimental density maps (dots) and the ratios of the numerical simulations (lines) where actin filaments can or cannot cross the dense actin network. Scale bars indicate 10 μm.

nucleation bar angles close to 22°, filaments are associated into short and thin antiparallel bundles. Parallel bundles only started to form above a critical angle between 22° and 45°, and averaged image analysis confirmed the existence of an optimal angle to promote the coalescence of numerous filaments into a parallel bundle (Fig. 3d).

As we had demonstrated that the length and rigidity of filaments modulate their interaction with actin-filament networks, we investigated whether or not a variation in the distance at a given angle between two nucleation regions would affect bundle formation. For this purpose we designed eight-branched radial arrays where the rays were moved in and out from the origin. As expected, filaments grew outward from each ray and formed parallel bundles on the bisecting line between adjacent rays (Fig. 4a,b, and see Supplementary Fig. S4). When rays were sufficiently distant, short parallel bundles formed precisely along the bisecting line and maintained this orientation. As the distance between rays decreased, bundles were longer, mis-positioned and curved (Fig. 4b,c). In all cases, the transition between the assembly of antiparallel bundles in the proximal part of the rays and the assembly of parallel bundles in their distal part occurred at a fairly variable position (Fig. 4d,e). Consequently, the distance between nucleation sites, in the range tested, was not critical to the generation of the final structure. The position of the transition from antiparallel to parallel bundles could be modelled as the result of intrinsic filament properties and collective assembly (Fig. 4f). If filaments assembled exclusively into antiparallel bundles in the proximal part of the network, filaments that contact one another would have a probability p to assemble into parallel bundles. This intrinsic probability p depends only on

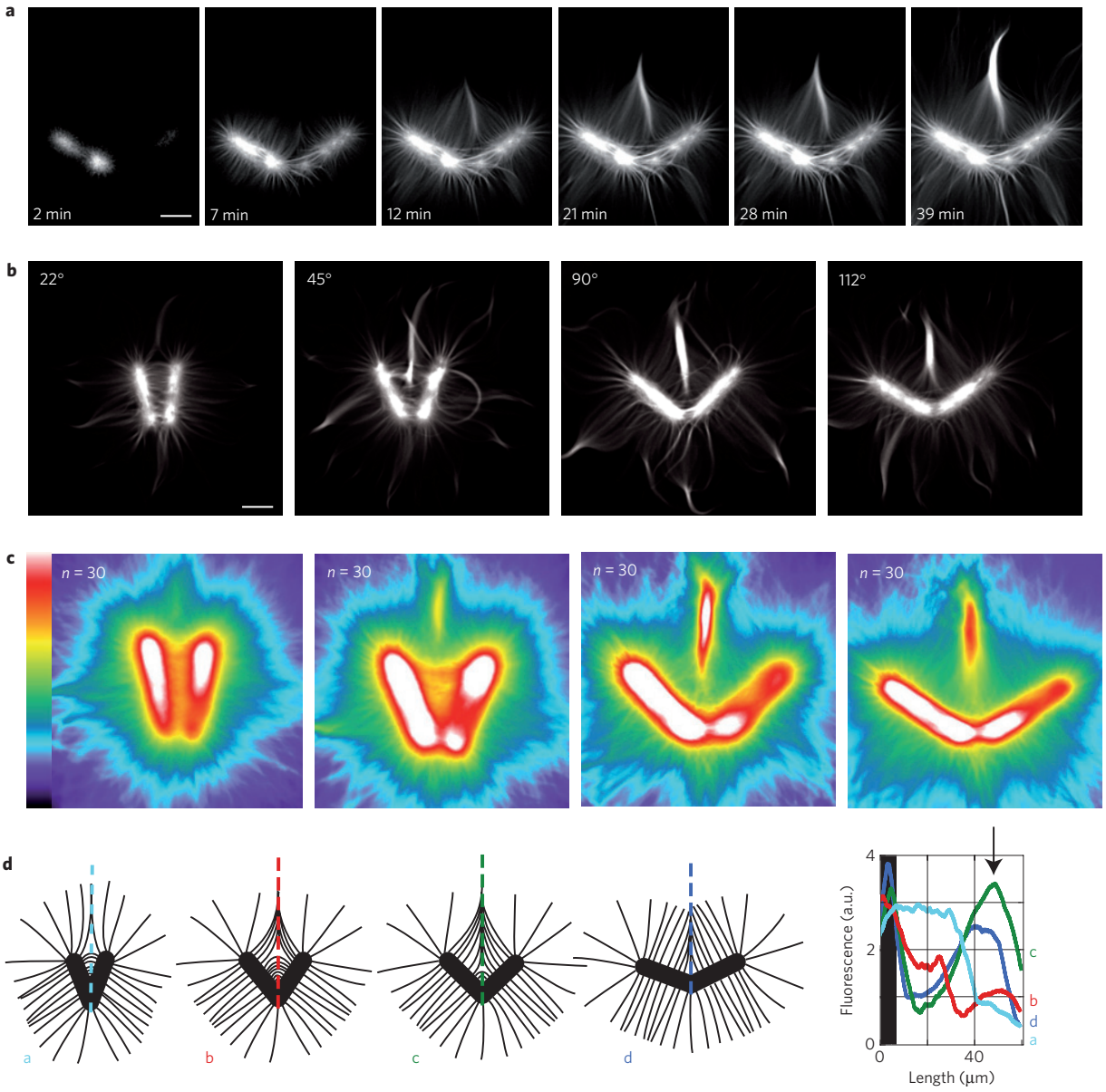

Figure 3 | Orientation of nucleation regions controls bundle formation. a, Nucleation, elongation and deformation of actin filaments nucleated on a 120° V-shaped nucleation zone. **b**, Fluorescence-microscopy images of actin structures formed on V-shaped zones with four different angles. **c**, Average fluorescent projection of 30 images for each angle. **d**, Schematic representation of bundle formation resulting from the interaction of actin filaments nucleated on the micropattern. The fluorescent-intensity distribution along the line scans (dotted lines) carried out on the averaged images relates the actin filament number involved in the bundle; the arrow, against curve c, indicates the maximum fluorescence corresponding to the bundle thickening at 45°. Scale bars indicate 10 μm. See also Supplementary Video S4.

filament orientation and therefore on their position along the ray (Fig. 1d and see Supplementary Fig. S5). If filaments formed a parallel bundle in the proximal network, the encountering filaments are forced to bend and contribute to this parallel bundle. Therefore the probability Q to form a parallel bundle is given by

$$Q(y+1) = p(y)(1-Q(y)) + Q(y)$$

which gives

$$Q(y) = 1 - \prod_{k=0}^{y-1}(1-p(k)) \qquad (1)$$

where y is a discrete variable characterizing the position along the bisecting axis (see Supplementary Equations). The transition positions obtained from the probability function Q precisely matched experimental data (Fig. 4g). As a transition point generates a parallel bundle made of all distal filaments, we calculated the bundle size and fluorescent intensity associated with each transition point (see Supplementary Equations). Our model accurately accounted for both the increase of fluorescence due to filament assembly into the bundle and the reduction of fluorescence due to various filament lengths within the bundle (Fig. 4h). These geometrically mediated bundles still occur in presence of two distinct actin cross-linkers in a concentration-dependent manner (see Supplementary Fig. S6 and Video S5). This confirms that bundle emergence is tightly controlled by mechanical properties of the actin filament[24].

Our reconstitution of the filopodium-like bundles relies on the spontaneous formation of a precursor structure formed by the collapse and the further coalescence of actin filaments emanating from

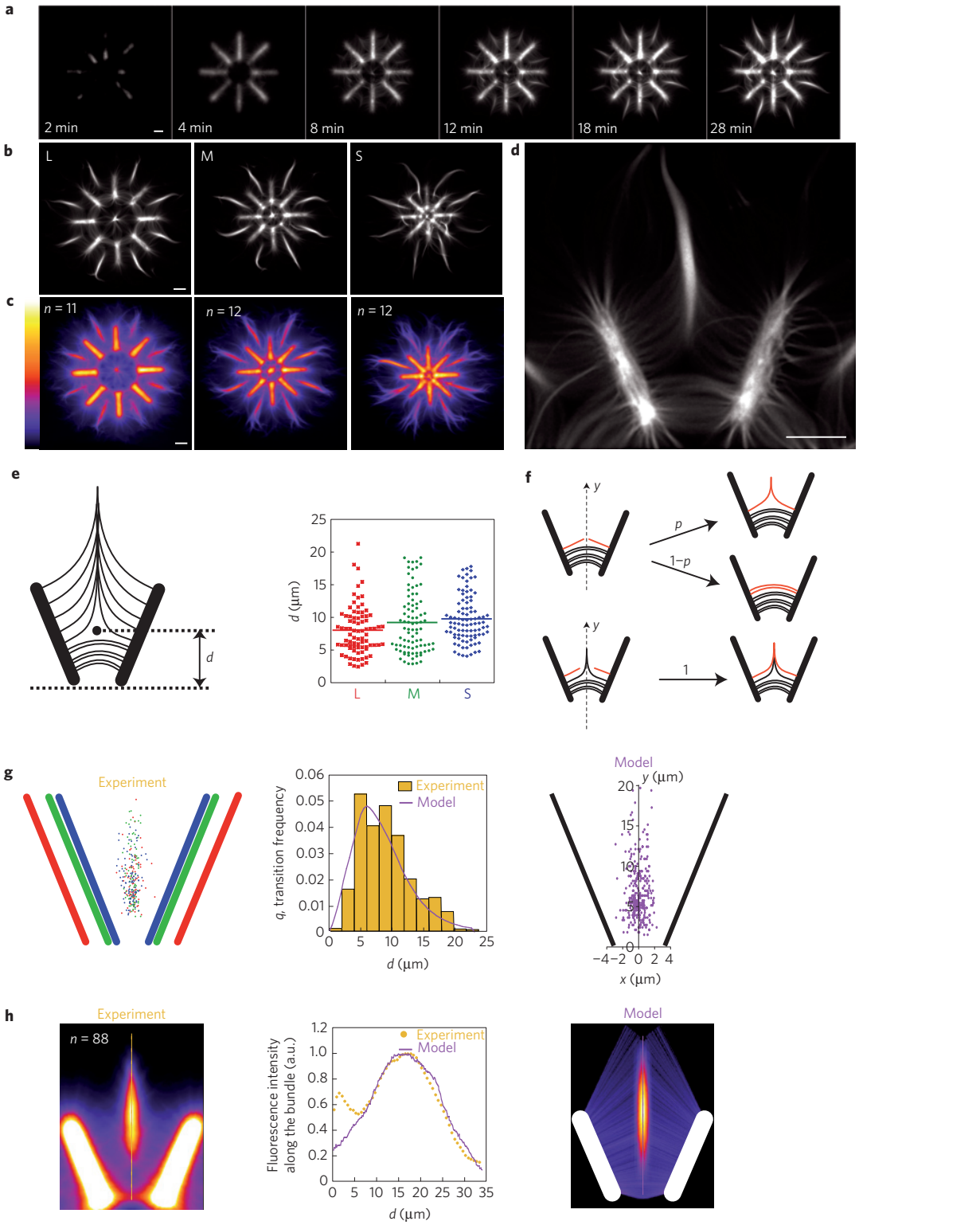

Figure 4 | Intrinsic properties and collective assembly of actin filaments regulate parallel-bundle formation. a, Time-lapse acquisition of the nucleation and elongation of actin filaments on an eight-branched radial array. **b**, Fluorescence images of three sizes of the radial array at steady state of actin assembly. **c**, Average fluorescent projections. **d** A zoom of the L-sized radial array of **b**. **e**, The distance *d* between the bottom of the bar and the position of the transition point did not vary between the three radial array sizes. **f**, Model assumptions: actin filaments' probabilistic comportment depends on their local environment. **g**, Left: combined experimental measures from **e** for the three different radial array sizes. Right: 200 transition-point positions calculated from the probability $Q(y)$ (equation (1)) and a normal variability along the *x* axis. Middle: comparison of experimental measures of the transition-point position and the model function $Q(y)$ (equation (1)). **h**, Left: average fluorescent projection of each sector of the large radial array. Right: the calculated fluorescent intensity of 10,000 parallel filaments constituting the bundle generated according to the function $Q(y)$. Middle: comparison of fluorescence intensity along the bisecting line on the experimental averaged image (dots) and on the analytical formulation obtained from the model. Scale bars indicate 10 μm.

the dense actin network, to which adjacent elongating filaments will systematically converge (see Supplementary Video S4). Interestingly, this propagative coalescence of actin filaments initiated by a precursor, such as the Λ-precursors corresponding to the splayed filopodial roots observed *in vivo*[6], accounts for the emergence of the parallel bundles from the dense surrounding network in cells. Moreover, this propagative process explains the presence of short actin filaments within bundles[25], consistent with the high barbed-end capping activity present at the leading edge of lamellipodia[26].

Our innovative methodology has demonstrated that, independently of the mixture of actin-binding proteins, nucleation geometry plays a key role in the determination of the actin-filament network architecture. Respective positioning of adjacent nucleation zones results in the entanglement of actin filaments into networks and the control of their length. Actin-filament orientation determines their ability to interact with neighbours and to form bundles. Fundamentally, basic mechanical and probabilistic laws govern the spatial arrangements of antiparallel and filopodium-like parallel filaments in response to defined geometrical boundary conditions. By extension to living cells, this work emphasizes the importance of the spatial and temporal organization of the nucleation areas, giving rise to specific actin-network architectures and hence controlling the location of force production. Although the spatio-temporal regulation of actin growth is known to influence cell shape[27,28], our work has revealed, in quantitative terms, that reciprocally physical boundaries, within or around the cell, control actin cytoskeleton architectures.

Methods

Micropatterning. Glass coverslips were oxidized with oxygen plasma (10 s, 30 W, Harrick Plasma, Ithaca, NY) and incubated with 0.1 mg ml^{-1} of polylysine-ι-*g*-polyethyleneglycol (JenKem Technology, TX) in HEPES 10 mM at pH 7.4 for 1 h. Pegylated coverslips were placed on a chromium synthetic-quartz photomask (Toppan Photomasks, Corbeil, France) using a home-made vacuum holder. The chromium layer of the photomask contained 3-μm-wide transparent micropatterns. The mask-covered coverslips were then exposed to deep ultraviolet light (l < 200 nm, UVO Cleaner, Jelight Company, Irvine, CA) for 5 min and coated with a solution of the nucleation promoting factor pWA at 0.5 μM for 15 min.

Actin polymerization. Protein mixtures were diluted in freshly prepared fluorescence buffer containing 10 mM imidazole-HCl (pH 7.8), 50 mM KCl, 1 mM $MgCl_2$, 100 mM dithiothreitol, 3 mg ml^{-1} glucose, 20 μg ml^{-1} catalase, 100 mg ml^{-1} glucose oxidase and 0.5% methylcellulose to induce actin polymerization. Actin polymerization was induced in a solution containing 2 μM actin monomers (7% labelled with Alexa568) and 6 μM profilin, and 30 nM Arp2/3 complex.

Image acquisition. Images were taken using an upright BX61 Olympus microscope equipped with a ×40 dry objective (UPLFLN, NA = 0.75), an XY motorized stage (Marzhauser, Germany) and a CoolSnap HQ2 camera (Roper Scientific, Germany). The microscope and devices were driven by MetaMorph (Molecular Devices, Downington, PA).

Image treatment. All images were taken using the same light intensity and exposure time. However, before being overlaid and averaged, image grey scales were adjusted to have the same minimum and maximum grey values. The images shown were filtered using the 'unsharp mask' and the 'Gaussian blur' filters from Image J software to highlight filaments from the background.

Received 18 March 2010; accepted 11 August 2010; published online 19 September 2010

References

1. Naumanen, P., Lappalainen, P. & Hotulainen, P. Mechanisms of actin stress fibre assembly. *J. Microsc.* **231,** 446–454 (2008).
2. Welch, M. D. & Mullins, R. D. Cellular control of actin nucleation. *Annu. Rev. Cell. Dev. Biol.* **18,** 247–288 (2002).
3. Chesarone, M. A., DuPage, A. G. & Goode, B. L. Unleashing formins to remodel the actin and microtubule cytoskeletons. *Nature Rev. Mol. Cell. Biol.* **11,** 62–74 (2010).
4. Hotulainen, P. *et al.* Defining mechanisms of actin polymerization and depolymerization during dendritic spine morphogenesis. *J. Cell. Biol.* **185,** 323–339 (2009).
5. Korobova, F. & Svitkina, T. Molecular architecture of synaptic actin cytoskeleton in hippocampal neurons reveals a mechanism of dendritic spine morphogenesis. *Mol. Biol. Cell.* **21,** 165–176.
6. Svitkina, T. M. *et al.* Mechanism of filopodia initiation by reorganization of a dendritic network. *J. Cell. Biol.* **160,** 409–421 (2003).
7. Vignjevic, D. *et al.* Role of fascin in filopodial protrusion. *J. Cell. Biol.* **174,** 863–875 (2006).
8. Loisel, T. P., Boujemaa, R., Pantaloni, D. & Carlier, M. F. Reconstitution of actin-based motility of Listeria and Shigella using pure proteins. *Nature* **401,** 613–616 (1999).
9. Theriot, J. A., Mitchison, T. J., Tilney, L. G. & Portnoy, D. A. The rate of actin-based motility of intracellular *Listeria monocytogenes* equals the rate of actin polymerization. *Nature* **357,** 257–260 (1992).
10. Welch, M. D., Rosenblatt, J., Skoble, J., Portnoy, D. A. & Mitchison, T. J. Interaction of human Arp2/3 complex and the *Listeria monocytogenes* ActA protein in actin filament nucleation. *Science* **281,** 105–108 (1998).
11. Bernheim-Groswasser, A., Wiesner, S., Golsteyn, R. M., Carlier, M. F. & Sykes, C. The dynamics of actin-based motility depend on surface parameters. *Nature* **417,** 308–311 (2002).
12. Cameron, L. A., Footer, M. J., van Oudenaarden, A. & Theriot, J. A. Motility of ActA protein-coated microspheres driven by actin polymerization. *Proc. Natl Acad. Sci. USA* **96,** 4908–4913 (1999).
13. Romero, S. *et al.* Formin is a processive motor that requires profilin to accelerate actin assembly and associated ATP hydrolysis. *Cell* **119,** 419–429 (2004).
14. Liu, A. P. *et al.* Membrane-induced bundling of actin filaments. *Nature Phys.* **4,** 789–793 (2008).
15. Achard, V. *et al.* A primer-based mechanism underlies branched actin filament networks formation and motility. *Curr. Biol.* **20,** 423–428 (2010).
16. Brieher, W. M., Coughlin, M. & Mitchison, T. J. Fascin-mediated propulsion of *Listeria monocytogenes* independent of frequent nucleation by the Arp2/3 complex. *J. Cell. Biol.* **165,** 233–242 (2004).
17. Haviv, L. *et al.* Reconstitution of the transition from lamellipodium to filopodium in a membrane-free system. *Proc. Natl Acad. Sci. USA* **103,** 4906–4911 (2006).
18. Vignjevic, D. *et al.* Formation of filopodia-like bundles *in vitro* from a dendritic network. *J. Cell. Biol.* **160,** 951–962 (2003).
19. Mogilner, A. & Rubinstein, B. The physics of filopodial protrusion. *Biophys. J.* **89,** 782–795 (2005).
20. Azioune, A., Storch, M., Bornens, M., Thery, M. & Piel, M. Simple and rapid process for single cell micro-patterning. *Lab Chip* **9,** 1640–1642 (2009).
21. Blanchoin, L. *et al.* Direct observation of dendritic actin filament networks nucleated by Arp2/3 complex and WASP/Scar proteins. *Nature* **404,** 1007–1011 (2000).
22. Machesky, L. M. *et al.* Scar, a WASp-related protein, activates nucleation of actin filaments by the Arp2/3 complex. *Proc. Natl Acad. Sci. USA* **96,** 3739–3744 (1999).
23. Mullins, R. D., Heuser, J. A. & Pollard, T. D. The interaction of Arp2/3 complex with actin: Nucleation, high affinity pointed end capping, and formation of branching networks of filaments. *Proc. Natl Acad. Sci. USA* **95,** 6181–6186 (1998).
24. Courson, D. S. & Rock, R. S. Actin crosslink assembly and disassembly mechanics for alpha-actinin and fascin. *J. Biol. Chem.* **285,** 26350–26357 (2010).
25. Medalia, O. *et al.* Organization of actin networks in intact filopodia. *Curr. Biol.* **17,** 79–84 (2007).
26. Iwasa, J. H. & Mullins, R. D. Spatial and temporal relationships between actin-filament nucleation, capping, and disassembly. *Curr. Biol.* **17,** 395–406 (2007).
27. Parker, K. K. *et al.* Directional control of lamellipodia extension by constraining cell shape and orienting cell tractional forces. *Faseb. J.* **16,** 1195–1204 (2002).
28. Thery, M., Pepin, A., Dressaire, E., Chen, Y. & Bornens, M. Cell distribution of stress fibres in response to adhesive environment geometry. *Cell. Motil. Cytoskeleton* **63,** 341–355 (2006).

Acknowledgements

We are grateful to C. J. Staiger, J. Plastino and D. Pellman for critical reading of the manuscript and suggestions. This work was supported by grants from Agence National pour la Recherche to L.B. (ANR-06-PCV1-0022 and ANR-08-BLAN-0012) and M.T. (ANR-08-JC-0103 and ANR-PCV08-322457); A-C.R. is supported by an IRTELIS fellowship from CEA.

Author contributions

A-C.R. and T.C. carried out the experiments. J-L.M. carried out the physical modelling. L.B., R.B-P. and M.T. directed the project and wrote the manuscript.

Additional information

The authors declare no competing financial interests. Supplementary information accompanies this paper on www.nature.com/naturematerials. Reprints and permissions information is available online at http://npg.nature.com/reprintsandpermissions. Correspondence and requests for materials should be addressed to R.B-P. or M.T.